Touch Induces Local Mechanical Strain in *C. elegans* Sensory Neurons

Adam L. Nekimken[1,2,†], Beth L. Pruitt[1,2,†,*], and Miriam B. Goodman[1,2,*]

[1]Stanford University Department of Mechanical Engineering
[2]Stanford University Department of Molecular and Cellular Physiology
[†]Current address: Fullmoon Sensors, Inc. (ALN) and University of California-Santa Barbara Department of Mechanical Engineering (BLP)
[*]Corresponding authors: blp@ucsb.edu (BLP) and mbgoodmn@stanford.edu (MBG)

December 28, 2019

Abstract

Cutaneous mechanosensory neurons are activated by mechanical loads applied to the skin likely to result in local mechanical strain within sensory neurons. Using a microfluidics device to deliver controlled stimuli to intact animals and large, immobile and fluorescent protein-tagged mitochondria as fiducial markers in the touch receptor neurons (TRNs), we visualized and measured touch-induced mechanical strain in *C. elegans* worms. At steady-state, touch stimuli sufficient to activate TRNs induce an average strain of 3.1% at the center of the actuator and that this strain decays to near zero at the edges of the actuator. We also measured strain in animals carrying mutations affecting links between the extracellular matrix (ECM) and the TRNs, but could not detect any differences in touch-induced mechanical strain between wild-type and mutant animals. Collectively, these results demonstrate that touching the skin induces local mechanical strain in intact animals and suggest that a fully intact ECM is not essential for transmitting mechanical strain from the skin to cutaneous mechanosensory neurons.

1 Introduction

The ability to sense mechanical stimuli is critical for the daily lives of animals, including humans. Eating, walking, and embracing loved ones all depend on

the sense of touch. Despite the importance of mechanical senses such as touch, hearing, and proprioception, the molecular mechanisms of mechanotransduction are poorly understand compared to chemical (smell, taste) and optical (vision) senses [Marshall and Lumpkin, 2012]. Recently, much of the research on mechanosensation has focused on understanding the workings of mechanically-gated ion channels that transduce a mechanical stimulus into an electrochemical signal. Understanding this process requires better understanding of how touch receptor neurons (TRNs) are deformed during touch in living animals.

Studying TRNs in humans or other mammals is difficult because of the variety of touch receptors, complexity of the skin, and the distributed nature of the sense of touch [Geffeney and Goodman, 2012]. To overcome these problems, we use the nematode *C. elegans* as a model organism due to its deterministic cellular lineage, widely available genetic techniques, and well-characterized nervous system [Altun and Hall, 2009]. The well-defined cell lineage ensures that the morphology and anatomical location of the TRNs are consistent among animals with the same genotype. The small size, translucent skin, and wide availability of stable transgenic lines with fluorescent labels further enable novel experiments with *C. elegans*. These characteristics make *C. elegans* ideal for research on touch sensation.

For a TRN to be activated during touch, it must be physically deformed in some way, at cellular or molecular scales. Force is perhaps a common quantity used to describe the strength of a mechanical perturbation, but measurement of force requires measuring the deformation of a calibrated standard. This additional calibration step thus requires some knowledge of the mechanical properties of the object being deformed, or of the mechanical properties of the stimulator. In the context of a biological specimen, it is rare to have sufficient information of the mechanical properties of a tissue, especially since biomaterials often exhibit non-linear and viscoelastic properties. Additionally, if we want to accurately measure the strength of the stimulus on a particular cell such as a touch neuron, we often cannot assume that the biological specimen has homogeneous mechanical properties because of the complex mechanical structure of biological cells.

Given these challenges, we typically rely on quantities that can be more directly measured, such as indentation, stretch, and mechanical strain. Using this approach, our prior work Petzold et al. [2013] showed that the magnitude of indentation is a better predictor of the probability of behavioral response than force in *C. elegans*. This finding is supported by subsequent studies that directly measured mechanosensory currents in TRNs using electrophysiology [Eastwood et al., 2015, Katta et al., 2019b] and has been incorporated into theoretical models of C. elegans touch sensation [Eastwood et al., 2015, Sanzeni et al., 2019]. These models posit that touch-induced mechanical strain in the TRNs leads to the activation of mechano-electrical transduction channels.

The predicted mechanical strain in TRNs has not been observed or measured directly. Here, we developed a method to visualize touch-induced mechanical strain and used to compare local mechanical strain in wild-type and mutant TRNs. Our approach uses fluorescent protein-tagged mitochondria expressed in

the TRNs to take the place of fluorescent beads typically used in traction force microscopy in cell-based assays [Ribeiro et al., 2016], enabling us to perform our measurements of TRNs in intact animals. It also depends on the TRN mitochondria being immobile on the time scale of the desired measurement. Fortunately, the TRNs are known to harbor large and immobile mitochondria that are distributed along their sensory [Sure et al., 2018]. Mitochondria have been used an imaging tool for evaluating neuronal mechanics in culture O'Toole et al. [2015]. To our knowledge, this is first application of mitochondria as mechanical fiducial markers in vivo and these are the first experiments to directly observe touch-induced strain in TRNs in living animals

2 Results

2.1 Measuring Mechanical Strain of TRNs

To directly measure touch-induced deformation of the TRNs, we applied mechanical stimuli to worms confined in a microfluidic device (Nekimken et al. [2017], Figure 1A). The microfluidic device has pneumatic actuators that consist of a thin flexible wall (10 µm thick, 50 µm tall, 50 µm wide) made of the elastomer polydimethylsiloxane (PDMS) that separates a channel filled with air from a worm in the trap channel. When air pressure in the actuator channel is increased using a pressure controller, the thin wall expands like a balloon, deforming the trapped worm and generating indentations sufficient to activate the TRNs Nekimken et al. [2017].

We selected worms that were oriented such that one of their ALM neurons received a stimulus from the devices actuator. Previous experiments using this device resulted in a lower frequency of ALM activation compared to AVM [Nekimken et al., 2017], which is probably due to the position of ALM with respect to the actuator. Although worms crawl on their lateral side, the rotational orientation of a worm in the devices trap varied. The magnitude of the deformation of the TRN depends on its position with respect to the middle of the actuator, which was outside of experimental control, resulting in a diversity of stimulus intensities. We were not able to choose worms whose TRNs were displaced a specific amount, since we could not measure this in real time, so we selected TRNs that deformed enough to observe visually during the experiment.

The one-dimensional mechanical strain in an object under pure tension or compression is defined as $\epsilon = \Delta L / L_0$, where L_0 is the original, undeformed length of an object, and ΔL is the change in length of the object when deformed. For our experiments, we used the distance between adjacent mitochondria in the TRN as the length to quantify the mechanical strain in the TRN between those mitochondria, as represented by the piecewise plot in Figure 1D. Previously, researchers inferred that touch-induced indentation of C. elegans creates mechanical strain in TRNs, but did not directly measure this strain [Eastwood et al., 2015, Katta et al., 2019b, Sanzeni et al., 2019]. Our method enables empirical observation of strain in C. elegans TRNs.

2.2 Touch sensitivity of transgenic worms

We performed a classical touch assay to assess the effect of the transgenic mitochondria marker on touch sensitivity. The assay involves stroking an eyebrow hair across a worm and observing its behavioral response. We compared the touch sensitivity of wild-type worms (N2) and the worms with the transgenic mitochondria marker (*jsIs1073*), which serve as the control for later experiments with transgenic mutants. We found no significant difference in touch sensitivity between these two strains (see Figure 2C, response probabilities of 0.869 and 0.865 for N2 and NM3573 (*jsIs1073*), respectively). The difference between the means was 0.00667 [95%CI -0.0347, 0.048]. Thus, we concluded that the transgene has no detectable effect on touch sensation.

2.3 Local indentation induces local mechanical strain in TRNs

Next, we considered the spatially averaged distribution of touch-induced strain in the TRN. The mitochondria are sparsely distributed in the TRN and strain is a pairwise measurement between adjacent mitochondria, so our strain measurements result in a series of discontinuous step functions for a single trial rather than a smooth curve (Figure 1D). Each segment of the plot indicates the average strain between the two markers, so the maximum local strain on each interval is likely larger than our measured strain. The average distance between mitochondria used as mechanical fiducial markers was 26 µm, the minimum distance was 5 µm, and the largest distance was 64 µm for experiments with control animals (see Table S1). We analyzed an average of 8.9 intervals per trial (see Table S2).

To align each trial to the center of the actuator, we interpolated the location of the actuators center in the longitudinal direction of the worm by fitting the deformation profile with a Gaussian distribution. We then assumed that the location of the maximum of the Gaussian fit is the longitudinal coordinate of the center of the actuator (see dotted line in Figure 1C). We took the average strain of all actuation events at each longitudinal position along the neurite (see Figure 2A). Because the head is less constrained in the microfluidic channel than other parts of the body, the measurements of displacement and strain on the anterior side of the actuator include both touch- and movement-induced mechanical strain on the neuron and, as a result, exhibit a larger variance.

As expected, greater deformation of the TRN, which is caused by deeper indentation, results in greater strain in the TRN (see Figure 2B). The magnitude of the stimulus received by the TRN depends in part on the rotational position of the worm with respect to the actuator. Because the actuator is fixed to the surrounding material of the device on all sides, its center is the location of maximum deformation. If the worm is rotated such that the neuron being imaged is close to the coverglass of the device, then its maximum deformation is less than if it was position at the middle of the actuator (see Figure 2D).

In our experiments, the average strain induced between the pair of mito-

chondria at the center of the actuator was 0.031 ±0.005 (mean ±SEM) for these animals. A linear regression fit indicates that the strain at the center of the actuator increases as a function of the maximum neuronal displacement according to $\epsilon = 0.0061x - 0.0067$, where ϵ is the strain and x is the maximum displacement. To our knowledge, these are the first *in vivo* measurements of touch-induced strain in touch receptor neurons.

2.4 Touch-induced mechanical strain in ECM mutants

Having measured touch-induced mechanical strain in TRNs, we hypothesized that the ECM around the TRN is necessary for inducing this strain when a touch stimulus is applied. To test this hypothesis, we measured touch-induced strain in worms with mutations affecting the ECM around the TRN.

Mutations in genes encoding ECM proteins linked to *C. elegans* TRNs cause multiple phenotypes. Some of these ECM mutants are partially or completely insensitive to touch. Others are unable to sense touch and no longer form the normal punctate distribution of mechano-sensitive ion channel complexes along the neurite. Without the key elements of this transduction complex in the proper location to sense mechanical stimuli, the TRNs are insensitive to touch.

Some ECM mutants also have positioning or attachment defects, in which the lateral TRNs remain close to their juvenile positions on the dorsal side of the animal rather than end up in the wild-type position on the lateral side of adult animals. In wild-type animals, the TRNs are engulfed by the hypodermal cells in this final location. In this context, the term attachment defect reflects the hypothesis that the TRNs are displaced from their juvenile position to their lateral location in wild-type adults due to mechanical attachments with surrounding cells.

While some mechanical coupling is by definition required to move the TRNs from their juvenile position, it is unknown what actually applies the force to move the neuron. Several genes are necessary for this process, but some may be involved in biochemical signaling pathways rather than applying mechanical forces. Additionally, it is not clear what is responsible for mechanical coupling of the TRN to its surroundings in wild-type adults once the TRN is in its final position. We hypothesized that strain transmission to the TRNs would be disrupted in animals with attachment defects.

To test this hypothesis, we measured touch-induced mechanical strain in ECM mutants. For the sake of clarity, we refer to these mutants using only the name of the mutant allele except where noted, but all worms used for strain measurements contain the same integrated transgene, *jsIs1073*. We chose mutants with a variety of these phenotypes to better understand which phenotypes correlate with mechanical coupling of the TRN to other tissues.

2.4.1 Touch-induced strain in animals with severe attachment defects

Disruption of *him-4* causes widespread tissue attachment defects to the point that some individuals display prolapse of the intestines out of the vulva [Vogel and Hedgecock, 2001]. *him-4(e1267)* mutants have TRN attachment defects and lack the distinct ECM around the TRNs [Vogel and Hedgecock, 2001]. Due to the large size of the *him-4* gene (36 kb), the *e1267* allele has not been previously annotated. To fill this knowledge gap, we determined the molecular nature of the allele using whole-genome sequencing. Using this approach, we determined that *e1267* encodes a frameshift caused by insertion of one base pair in the third intron of the *him-4* gene (see Figure S1). A second polymorphism was detected in the intron following the 48th exon. Based on our whole-genome sequencing and the prior genetic studies of *him-4(e1267)*, we conclude that the *e1267* allele is a null allele.

Because *him-4(e1267)* null mutants retain some touch sensitivity and grossly normal MEC-4 puncta Emtage et al. [2004], we this mutant to test whether severe attachment defects affect transmission of strain to TRNs, and, if the attachment defect does affect strain transmission, whether this could account for the decrease in touch sensitivity. In parallel, we also performed touch assays of *him-4(e1267)* null mutants and detected a minor defect in touch sensation (Table 1). We tracked an average of 9.1 mitochondria with an average distance between adjacent mitochondria of 28 µm for *him-4(e1267)* animals (see Tables S1 and S2 for comparison with control animals). We found that touch-induced strain in *him-4(e1267)* animals is effectively the same as in control animals: mean difference of -0.007 with a 95% confidence interval of (-0.020, 0.007) (see Figures 3 and 4 and Table 2). Collectively, these findings suggest that *him-4*-induced defects in TRN positioning play a minor role in touch sensation and, within the resolution of our measurements, in the generation of touch-induced mechanical strain.

2.4.2 Strain transmission in _Mechanosensory abnormal mutants with attachment defects

Next, we sought to understand strain transmission in mutants that are insensitive to touch (see Table 1). Some _Mec mutants have attachment defects in addition to disruptions in organization of the mechano-sensitive ion channel complex. Two genes that code for extracellular proteins, *mec-1* and *mec-5*, were identified as part of an early mutagenesis screen for touch-insensitive mutants [Chalfie and Sulston, 1981]. Knocking out these genes results in a loss of the characteristic electron-dense ECM that is visible around the TRNs in electron micrographs.

MEC-1 is an ECM protein produced by the TRNs with two EGF domains and 15 Kunitz-like domains. *mec-1* null mutants do not form the punctate distribution of MEC-4 ion channel complexes along the TRN neurite [Emtage et al., 2004]. Some, but not all, *mec-1* mutants that are insensitive to touch also

have defects in TRN positioning or attachment [Emtage et al., 2004], suggesting that the two functions of the protein are independent. It is possible, therefore, that MEC-1 is necessary for transmission of mechanical stimuli to the TRNs in addition to being necessary for organization of the ion channel complex.

MEC-5 is a collagen produced by hypodermal cells that engulf the lateral TRNs in wild-type worms, and it is necessary for touch sensation [Du et al., 1996]. *mec-5* null mutants may have attachment defects, but not to the same extent as those in *mec-1* or *him-4* mutants. Instead of remaining in their juvenile position next to the muscle as in other mutants with more severe attachment defects, the neurites of TRNs in *mec-5* null mutants meander, with some parts of the neurite close to the muscle and other parts closer to the position of wildtype TRNs [Emtage et al., 2004]. MEC-5 is also necessary for formation of the punctate distribution of the mechanosensitive ion channels *mec-5* mutants.

The defects in MEC-4 puncta are presumed to account for the loss of touch sensation in *mec-1* and *mec-5* mutants. We hypothesized that these mutants would have defects in the generation touch-induced mechanical strain that correlated with defects in TRN attachment. In this scenario, touch-induced mechanical strain would be impaired in mutants with defects in TRN attachment, but not those with normal TRN positioning and attachment. To test this idea, we chose two mutant alleles of *mec-1* with different phenotypes. The *e1738* allele encodes a premature stop codon and causes a loss of touch sensitivity, but displays normal attachment of the TRN. The *e1066* allele, by contrast, causes both loss of touch sensation and disruption of attachment. The *mec-5(u444)* allele comprises a deletion of a large portion of the gene and is presumed to be a null allele

We tested these hypotheses by measuring mechanical strain in these ECM mutants (see Tables S1 and S2 for comparison of number of mitochondria and distance between adjacent mitochondria with control animals). Our results indicate that the hypothesis that attachment defects correlated with reduced strain transmission is incorrect (see Figure 3). There is effectively no difference between control and *mec-1(e1738)*, *mec-1(e1066)*, or *mec-5(u444)* animals 4 and Table 2). Thus, these ECM proteins are dispensable for touch-induced strain in TRNs as measured by the deformation between adjacent mitochondria.

3 Discussion

3.1 Local indentation causes local strain in *C. elegans* TRNs

Transduction of a mechanical stimulus to an electrical or biological signal requires deformation of a sensing element. For this element to deform, the mechanical stimulus must be transmitted to it from the surroundings. In the case of *C. elegans* touch sensation, ion channels transduce mechanical stimuli into electrical signals in the TRNs [O'Hagan, 2005], but how the stimulus is transmitted to the channels is unknown. We created a method for characterizing

the deformation of the TRNs so we could better understand how TRNs are activated.

Using mitochondria as fiducial markers in *C. elegans* TRNs, we showed for the first time that local indentation of the body of a worm leads to local strain in its TRNs. The magnitude of this strain is dependent on the depth of indentation of the TRN. In wild-type animals, the touch-induced strain closest to the point of maximum indentation was 0.031 $\pm$0.005 (mean $\pm$SEM).

Previous studies reported complementary measurements of the strain in *C. elegans* TRNs by measuring the change in length of the entire neuron during locomotion [Krieg et al., 2014]. In this case, the TRN is subjected to strains on the order of $\pm$0.4 without apparent damage [Krieg et al., 2014]. Given that the touch-evoked TRN strain is an order of magnitude smaller than this value, the touch-evoked strains are well within the ability of the TRNs to experience without damage. The TRNs are not activated by the gobal mechanical strain induced by normal locomotion for several reasons. For instance, locomotion-induced strain occurs slowly, too slowly to activate the TRNs [Eastwood et al., 2015, Katta et al., 2019b].

Our technique may underestimate the mechanical strain induced by touch stimuli. Consistent with the idea that the strain measured in this study constitutes a lower bound on the true values, simulations Sanzeni et al. [2019] indicate that indentation by a spherical bead induces strain along the longitudinal dimension of the worm with a magnitude of approximately 0.12. Because this value comes from a simulation, the strain is calculated from a continuous deformation function, so there is no averaging due to spatial limitations. The magnitude of the one-dimensional strain in our measurements may be less than computational estimates of strain due to reduced spatial resolution and a different stimulus paradigm.

Additionally, the simulations by Sanzeni et al. [2019] indicate that strains of similar magnitude are present in the other two dimensions (along the direction of the stimulus and tangential to the circumference of the worm at the point of the stimulus). Due to the nature of our measurement, we were only able to measure one-dimensional strain along the length of the TRN, so we have little information about the strains in different directions. Our measurements of touch-induced strain can be incorporated into future models of *C. elegans* touch sensation, which may improve our understanding of the mechanical state of the TRN and mechano-sensitive ion channel complex upon touch stimulation.

3.2 Strain transmission and touch sensitivity of ECM mutants

We hypothesized that the ECM of the TRNs would be involved in transmitting stimuli to the TRN. As a result, we predicted that touch sensitivity would be correlated with ECM-mediated transmission of mechanical strain to the TRNs.

The purpose of measuring strain transmission in *him-4* mutants was to test this hypothesis, because *him-4* mutants have widespread tissue attachment defects but are still sensitive to touch stimuli. Although *him-4(e1267)* mutants

are less sensitive to touch than control animals (Table 1), they still respond on average to more than half of the touches applied by an eyebrow hair. This finding and the observation that MEC-4 still localizes to puncta in *him-4* mutants suggest that the mechano-electrical transduction complex retains its function, but exhibits reduced sensitivity to external touch. We reasoned the decrease in sensitivity might reflect a decrease in touch-induced mechanical strain. No such effect could be detected, however, indicating TRN attachment plays a surprisingly minor role in the transmission of mechanical energy from the skin to the sensory neuron.

In contrast, *mec-1(e1066)*, *mec-1(e1738)*, and *mec-5(u444)* mutants have severe touch defects (Table 1). The mechano-electrical transduction complex does not form its normal punctate distribution in these mutants [Emtage et al., 2004], so they are likely touch-insensitive because they lack the proper transduction complex. As a result, differences in touch-induced strain in the TRNs of these animals dont explain their touch-insensitivity. Instead, we sought to test whether MEC-1 and MEC-5 have the additional function of transmitting strain to the TRNs. We also found no significant difference in touch-induced strain among the mutants we tested. Based on our results, it is likely that explicit ECM attachments are not necessary for local deformation of the TRNs.

3.3 Other sources of mechanical coupling

Here, we report that touch-induced mechanical strain in the TRNs is independent of their attachement to other tissues or the expression of ECM proteins MEC-1 and MEC-5, at least at steady state. This finding implies that mechanical coupling between the skin and sensory neurons remains in mutants with ECM defects.

One alternative source of mechanical coupling is friction between the TRN and surrounding tissues. In this scenario, all of the worm's tissues are compacted together by a high hydrostatic pressure and this would be expected to elevate friction between tissues. Further compression applied to the outside of the worm during touch stimulation could lead to stiffening of the worms body that might be caused by internal structures jamming together [Gilpin et al., 2015]. When we and others immobilize worms in microfluidic devices, we fabricate channels small enough to apply gentle compressive forces that the worm cannot overcome. As a result, the worm is compressed on all sides except the nose and tail when in the microfluidic trap, potentially jamming the TRNs against surrounding tissues and further increasing friction. Another possibility is that the generation of touch-induced local mechanical strain is dominated by the cytoskeleton. In support of this idea, mutations that discrupt the microtubule cytoskeleton and actin-spectrin networks lead to compression-induced shape defects and impaired touch sensation Krieg et al. [2017, 2014]. Additionally, loss of genes encoding alpha and beta tubulin decrease mechanoreceptor currents and increase stimulus amplitude needed to activate these currents O'Hagan [2005], Bounoutas et al. [2009]. Additional experimental work will be needed to differtiate among these possibilities.

3.4 Spatial scale of mechanical strain transmission

It is also possible we did not detect a change in strain transmission efficiency for technical reasons. Other research shows that the ECM does have some impact on mechanical coupling of the TRNs to their surroundings. In particular, the effects of mutations in cytoskeletal genes can be enhanced by mutations in the ECM. Cutting the TRN with a laser axotomy allows the cut ends of the axon to retract about 0.5 µm on average, releasing the constitutive tension in the TRN [Krieg et al., 2014]. This retraction distance increased by approximately 0.5 µm with the addition of a *him-4(e1267)* mutation. This result suggests that attachment to the TRNs of *him-4(e1267)* mutants is disrupted, allowing them to retract marginally farther when the TRN is cut, releasing more of the tension in the TRN. The larger retraction distance indicates that the spatial extent of the strain induced in the TRN of a *him-4(e1267)* mutant would be smaller than in a wild-type animal because the TRN has reduced mechanical coupling to the surrounding tissue, and the strain is transmitted less efficiently.

Our experiments, however, may not be able to detect this difference due to limited spatial resolution. The spatial resolution of our strain measurements is dictated by the location of mitochondria in the TRN. Because the retraction of axotomized *him-4(e1267)* TRNs presented by Krieg et al. [2014] averaged only 1 µm and the average distance between adjacent mitochondria for all of our strain measurements was 26 µm, that change in strain transmission may have been too small for us to detect. There may be other defects that we were unable to detect due to limited spatial resolution.

3.5 Strain-rate dependence

Other experiments have shown that wild-type *C. elegans* TRNs are activated mostly by high-velocity stimuli [Suzuki et al., 2003, Eastwood et al., 2015, Nekimken et al., 2017, Katta et al., 2019b]. Because of the time required to acquire a z-stack, we can only measure TRN strain at steady-state and are unable to evaluate how mechanical strain is affected by varitions in stimulus speed. This leaves open the possiblity that the ECM mutants we tested affect the dynamics of TRN deformation. In particularly, if disrupting the ECM of the TRN reduces the elastic component of the connections to the surrounding tissues, these mutations could further reduce the sensitivity of the TRN to lower strain rates by making the viscous component more prominent. Thus, the time to acquire z-stacks may have prevented us from observing changes in the dynamics of TRN deformation in ECM mutants.

3.6 Improving strain measurement *in vivo*

We used labelled mitochondria as fiducial markers and a microfluidics chip for delivering touch-like stimuli, enabling the first direct visualization of touch-induced mechanical strain in the TRNs. This approach has limited temporal and spatial resolution, however. Temporal resolution would be improved by

using faster imaging techniques. Ideally, volumes would be acquired at 20 Hz or faster, making it possible to observe mechanical strain in a 10 Hz buzz stimulus that we previously used to activate the TRNs [Nekimken et al., 2017]. Another approach would be to forgo volumetric imaging entirely and exclude trials with significant deformation and movement along the optical imaging axis.

The spatial resolution of strain measurements could be improved by using a more closely spaced fiducial markers. This would improve spatial resolution but could also make image analysis more difficult. If the fiducial markers are close together in a somewhat regular pattern, it is difficult to track where individual markers go in subsequent images. From an image analysis perspective, an ideal fiducial marker would have either a random distribution, enabling tracking by pattern correlation, or a sparse enough distribution that individual particles can be followed. While the mitochondria are bright and mechanically stable, the distance in between adjacent mitochondria is more than 20 µm (Table S1).

One promising candidate for fiducial markers in future experiments is fluorescently-tagged MEC-4. When we performed our experiments, the available MEC-4 tags were too dim, but newer strains have much brighter MEC-4 tags [Katta et al., 2019a]. Assuming a reliable image analysis method is available, MEC-4 tags would be ideal, since a major goal of the measurement is to understand the mechanical stimulus received by the MEC-4 channel complex. These improvements in temporal and spatial resolution may yield additional insights in the process of mechanical strain transmission to TRNs.

4 Conclusion

We have performed the first *in vivo* measurements of touch-induced mechanical strain in *C. elegans* TRNs. We used mechanically-stable mitochondria in the TRNs to observe deformation of the TRN and found that local touch stimuli applied in a microfluidic device induces local strain in the TRN. Defects in the ECM surrounding the TRN did not alter the mechanical strain in the TRN, indicating that explicit attachments are not necessary for deformation of the TRN. Further experiments using our method to study mutants with defects in other structures, such as the cuticle or hypodermal cells, might show which structures are responsible for deformation of the TRNs. Our method can also be used to measure mechanical strain in other neurons, providing a new tool for experimental investigation of the mechanics of *in vivo* neurons.

5 Methods and Materials

5.1 Nematode strains

For all experiments measuring mechanical strain, we used animals carrying *jsIs1073*[pmec-7::TagRFP-mito::CBunc-119], a transgene that drives expression of TagRFP in the mitochondria in the TRNs [Zheng et al., 2014]. We crossed this worm strain with other strains containing the mutant alleles we wanted to

test (see Table 6). We confirmed crosses by sequencing to ensure the progeny of each cross were homozygous for the expected mutant allele (see Table S3 for primer sequences) and by imaging to confirm that all progeny were homozygous for the transgenic fluorescence marker. For *him-4(e1267)*, we initially confirmed the cross by observing the vulva prolapse and premature death of adults, then later confirmed the mutation with sequencing after we characterized the molecular nature of the allele with whole-genome sequencing.

5.2 Microfluidic immobilization and mechanical stimulation

To provide a repeatable mechanical stimulus that is compatible with imaging the mitochondria of the TRN, we used a microfluidic device made of the transparent elastomer PDMS for simultaneous mechanical stimulation and imaging of *C. elegans* [Nekimken et al., 2017]. Using an Elveflow OB1 pressure controller, we applied pressure to one of the devices actuators to create a mechanical stimulus. We fabricated and operated devices designed for use with young adult worms as described in Nekimken et al. [2017] and Fehlauer et al. [2018]. Because worms immobilized in this trap are uniformly and partially deformed by the channel, we refer to this as the rest configuration.

5.3 Sample preparation

We performed all experiments using young adult animals that were synchronized three days before the experiment using hypochlorite treatment, then cultured them on agar plates with OP50 bacteria for food. We transferred animals from the agar plates with a platinum wire pick to a small petri dish containing the medium we use to carry worms in the polydimethylsiloxane (PDMS) microfluidic device.

This medium was a mixture of saline and iodixanol, a non-toxic density gradient medium [Boothe et al., 2017]. By using an immersion medium with the same refractive index as PDMS, we minimized reflections and refractions that disrupted fluorescence imaging. Physiological saline is the same as that used for electrophysiological recordings from *C. elegans* neurons O'Hagan et al. [2005] and contained (in mM): NaCl (145), KCl (5), $MgCl_2$ (5), $CaCl_2$ (1), and Na-HEPES (10), adjusted to a pH of 7.2 with NaOH. To obtain a final medium that was 30% saline and 70% Optiprep with a refractive index of 1.4, we mixed saline with with Optiprep (Sigma Aldrich, a 60% (w/v) solution of iodixanol in water). The final immersion medium has an osmolality of 300-325 mOsm (Fiske Micro-Osmometer Model 210), so it does not cause large osmotic shocks to *C. elegans*. By contrast with other fluids we tested (e.g. glycerol, halocarbon oil), this medium has a viscosity that is only slightly higher than physiological saline.

During the picking step, we selected animals so they fit in the microfluidic trap with minimal movement but could also be ejected through the narrow opening at the head of the trap. When performing experiments with *him-4*

mutants, we chose animals whose gross morphology was wild-type and avoided animals whose intestines were everted.

After using the pick to push away large particles that might clog the microfluidic device, we aspirated the worms into polyethylene tubing (Intramedic tubing size PE50, BD) with a syringe (1 mL Luer-Lok, BD) and connected the tubing to the devices inlet. For each trial, we pushed a worm into the trap channel using the syringe and then evaluated whether to use this worm for an experiment based on our inclusion criteria.

5.4 Imaging

Although the mechanical stimulus is mostly in the horizontal direction, there is enough deformation in the z-direction to move the neuron out of plane during stimulation in some cases. In initial experiments with a traditional epifluorescence microscope, the mitochondria often moved out of focus during stimulation due to movement in the z-direction. To account for this problem, we used a spinning disk confocal microscope (Nikon TiE, Yokogawa CSU-X1, 40x/NA 1.4 oil objective, and Photometrics Prime95B sCMOS camera) to acquire z-stacks, which provided adequate resolution in the z-direction.

For each trial, we acquired 11 z-stacks containing the neuron of interest, with 300 kPa of pressure applied during the even-numbered stacks, and 0 kPa applied during the odd-numbered stacks. We started acquisition of a stack every 15 seconds, although the time to acquire each given stack was approximately 12 seconds. During the short delay between acquisition of stacks, we toggled the applied pressure. The exact time varied depending on the height of the z-stack, which was manually set to accommodate observed motion in the z direction during the test actuation.

5.5 Inclusion criteria for imaging trials

The microfluidics device is designed for young adult hermaphrodites and animals that were too small are not sufficiently immobilized and were flushed from the channel without imaging. Further, we focused our data collection on animals with their TRNs oriented adjacent to the stimulating channels, optimizing the subsequent mechanical stimluation.

5.6 Image analysis

To detect the mitochondria, we used a python implementation [Allan et al., 2018] of a particle-tracking algorithm originally presented by Crocker and Grier [Crocker and Grier, 1996]. Briefly, the algorithm involves applying a spatial band pass filter, finding peaks, refining the position of peaks by finding their center of mass, and linking particles across timepoints into trajectories.

For some stacks, the algorithm failed to detect the mitochondria because they were too close to the top or bottom of the stack, were not bright enough, overlapped with the mitochondria of another TRN, or were blurred due to the

motion of the worm. We discarded all stacks subsequent to a stack where the image processing failed, because the strain measurement requires comparison to a previous stack. Additionally, not all of the stacks from each trial were usable, since the fluorophores bleached over time. As a result, not all actuation events yielded strain measurements (see Supplementary Figure S2).

Due to variability across trials, we manually selected a region of interest around the TRN and tuned parameters in the particle tracking algorithm. Primarily, we changed the minmass threshold, which filters out particles where the sum of pixel values within the boundaries of the particle is below the chosen threshold, and the search radius for the linking step, which specifies how far a particle can travel between timepoints and still be identified as the same particle. Less frequently, we changed the cutoff size for the bandpass filter or the brightness percentile threshold, which sets a minimum value for the brightest pixel in a particle as a percentile of the brightness of pixels in the image. We tuned these parameters until the particles found and linked included only particles along the location of the neuron and not autofluorescent spots. Supplemental Figure S3 shows the range of parameters we used.

5.7 Touch assays

To test the touch-sensitivity of the mutants used in our strain transmission experiments, we performed touch assays by lightly stroking an eyebrow hair across the body of a worm and scoring its behavioral response [Goodman, 2006]. For each session of touch assays, we tested 25 worms from a plate, performing 10 touches per worm. We performed the touch assays blinded with respect to genotype. For each touch event, we counted a response consisting of reversing direction or speeding up to move away from the stimulus as a positive response.

5.8 Whole-genome sequencing of *him-4(e1267)*

Our whole-genome sequencing protocol involved four sub-protocols: DNA extraction, sequencing library preparation, sequencing, and analysis. We isolated DNA from CB1267 (him-4(e1267) X) with a phenol chloroform isoamyl alcohol (PCI) extraction. First, we washed the worms off a mostly starved plate using M9, rinsed in clean M9 twice, resuspended in EN buffer, removed the supernatant, and flash-froze the sample in liquid nitrogen. Next, we added 450 µL of worm lysis buffer (0.1 M TRIS pH 8.5, 0.1 M NaCl, 50 mM EDTA, and 1% SDS) and 40 µL of proteinase K to 50 µL of frozen worms and incubated at 62°C for 45 minutes, vortexing occasionally. Then, we performed the PCI extraction in a phase lock gel tube (VWR) by adding 500 µL of PCI to the sample, vortexing, spinning for 5 minutes at 10,000 rpm, and then collecting the upper phase. We repeated the PCI extraction step, and then extracted two more times using chloroform. We precipitated the DNA by adding 40 µL of 5 M sodium acetate and 1 mL of ethanol, spinning for 5 minutes at 10,000 rpm, removing the supernatant, washing in 70% ethanol, and resuspending in 50 µL of TE buffer at pH 7.4.

We created a sequencing library according to manufacturer instructions using the Nextera DNA Library Prep Kit from Illumina. Briefly, this includes tagmentation of the DNA using the Illumina Tagment DNA Buffer and Enzyme, clean-up of the tagmented DNA using a Zymo DNA Clean and Concentrator Kit, PCR to add the library indices to the tagmented DNA, and PCR cleanup by gel extraction using a Qiagen MinElute Kit. We did a quality control step using the Agilent Bioanalyzer at the Stanford Protein and Nucleic Acid Biotechnology Facility. The sequencing was completed on an Illumina NextSeq sequencer in the Stanford Functional Genomics Facility.

We analyzed the sequencing data using the computing cluster of the Stanford Center for Genomics and Personalized Medicine. Briefly, we mapped reads using Bowtie2, used Picard to sort reads, mark duplicates, and prepare read groups, then used GATK to select high quality SNPs and INDELs, and SnpEff to annotate the results. The complete script used for this analysis is available at `https://github.com/anekimken/whole_genome_sequencing`.

6 Acknowledgments

We thank Chloe Girard, Chantal Akerib, Melissa Pickett, and Anne Villenueve for assistance with whole genome sequencing; Michael Nonet for the gift of NM3573, the strain with labeled mitochondria in the TRNs; Ehsan Rezeai for help with software testing.

Some of the experiments were performed at Stanford core facilities, including the Cell Sciences Imaging Facility, Functional Genomics Facility (funded in part by a Shared Instrumentation Grant, NIH S10OD018220), the Genetics Bioinformatics Service Center, and the nano@Stanford labs (supported by the National Science Foundation as part of the National Nanotechnology Coordinated Infrastructure under award ECCS-1542152).

This work was funded by an NIH fellowship to ALN (F31NS100318) and grant to MBG (R35NS105092).

References

D. B. Allan, T. Caswell, N. C. Keim, and C. M. van der Wel. trackpy: Trackpy v0.4.1, 4 2018. URL https://doi.org/10.5281/zenodo.1226458#.XUn7KiB2xhk.mendeley.

Z. F. Altun and D. H. Hall. Introduction. *WormAtlas*, 26(3):619–631, 2009. ISSN 08966273. doi: 10.3908/wormatlas.1.1.

T. Boothe, L. Hilbert, M. Heide, L. Berninger, W. B. Huttner, V. Zaburdaev, N. L. Vastenhouw, E. W. Myers, D. N. Drechsel, and J. C. Rink. A tunable refractive index matching medium for live imaging cells, tissues and model organisms. *eLife*, 6, 7 2017. ISSN 2050-084X. doi: 10.7554/eLife.27240. URL https://elifesciences.org/articles/27240.

A. Bounoutas, R. O'Hagan, and M. Chalfie. The Multipurpose 15-Protofilament Microtubules in C. elegans Have Specific Roles in Mechanosensation. *Current Biology*, 19(16):1362–1367, 8 2009. ISSN 09609822. doi: 10.1016/j.cub.2009.06.036. URL http://dx.doi.org/10.1016/j.cub.2009.06.036https://linkinghub.elsevier.com/retrieve/pii/S0960982209013128.

M. Chalfie and J. Sulston. Developmental genetics of the mechanosensory neurons of Caenorhabditis elegans. *Developmental Biology*, 82(2):358–370, 3 1981. ISSN 00121606. doi: 10.1016/0012-1606(81)90459-0. URL http://linkinghub.elsevier.com/retrieve/pii/0012160681904590.

J. C. Crocker and D. G. Grier. Methods of Digital Video Microscopy for Colloidal Studies. *Journal of Colloid and Interface Science*, 179(1):298–310, 4 1996. ISSN 00219797. doi: 10.1006/jcis.1996.0217. URL https://linkinghub.elsevier.com/retrieve/pii/S0021979796902179.

H. Du, G. Gu, C. M. William, and M. Chalfie. Extracellular proteins needed for C. elegans mechanosensation. *Neuron*, 16(1):183–194, 1996. ISSN 08966273. doi: 10.1016/S0896-6273(00)80035-5.

A. L. Eastwood, A. Sanzeni, B. C. Petzold, S.-J. Park, M. Vergassola, B. L. Pruitt, and M. B. Goodman. Tissue mechanics govern the rapidly adapting and symmetrical response to touch. *Proceedings of the National Academy of Sciences*, 15(50):E6955–E6963, 12 2015. ISSN 0027-8424. doi: 10.1073/pnas.1514138112.

L. Emtage, G. Gu, E. Hartwieg, and M. Chalfie. Extracellular proteins organize the mechanosensory channel complex in C. elegans touch receptor neurons. *Neuron*, 44:795–807, 2004. ISSN 08966273. doi: 10.1016/j.neuron.2004.11.010.

H. Fehlauer, A. L. Nekimken, A. A. Kim, B. L. Pruitt, M. B. Goodman, and M. Krieg. Using a Microfluidics Device for Mechanical Stimulation and High Resolution Imaging of ¡em¿C. elegans¡/em¿. *Journal*

of Visualized Experiments, (132):e56530–e56530, 2 2018. ISSN 1940-087X. doi: 10.3791/56530. URL https://www.jove.com/video/56530/using-microfluidics-device-for-mechanical-stimulation-high-resolution.

S. L. Geffeney and M. B. Goodman. How We Feel: Ion Channel Partnerships that Detect Mechanical Inputs and Give Rise to Touch and Pain Perception. *Neuron*, 74(4):609–619, 2012. ISSN 08966273. doi: 10.1016/j.neuron.2012.04.023. URL http://dx.doi.org/10.1016/j.neuron.2012.04.023.

W. Gilpin, S. Uppaluri, and C. P. Brangwynne. Worms under Pressure: Bulk Mechanical Properties of C. elegans Are Independent of the Cuticle. *Biophysical Journal*, 108(8):1887–1898, 4 2015. ISSN 00063495. doi: 10.1016/j.bpj.2015.03.020. URL https://linkinghub.elsevier.com/retrieve/pii/S0006349515002817.

M. Goodman. Mechanosensation. *WormBook*, pages 1–14, 2006. ISSN 15518507. doi: 10.1895/wormbook.1.62.1. URL http://www.wormbook.org/chapters/www_mechanosensation/mechanosensation.html.

S. Katta, A. Sanzeni, A. Das, M. Vergassola, and M. B. Goodman. Progressive recruitment of distal MEC-4 channels determines touch response strength in C. elegans. *The Journal of General Physiology*, 151 (10):1213 LP – 1230, 10 2019a. doi: 10.1085/jgp.201912374. URL http://jgp.rupress.org/content/151/10/1213.abstract.

S. Katta, A. Sanzeni, M. Vergassola, and M. B. Goodman. Progressive recruitment of distal MEC-4 channels determines touch response strength in C . elegans. *bioRxiv*, 2019b. doi: 10.1101/587014. URL https://www.biorxiv.org/content/10.1101/587014v1.

M. Krieg, A. R. Dunn, and M. B. Goodman. Mechanical control of the sense of touch by β-spectrin. *Nature Cell Biology*, 16(3):224–233, 2014. ISSN 1465-7392. doi: 10.1038/ncb2915. URL http://www.nature.com/doifinder/10.1038/ncb2915.

M. Krieg, J. Stühmer, J. G. Cueva, R. Fetter, K. Spilker, D. Cremers, K. Shen, A. R. Dunn, and M. B. Goodman. Genetic defects in β-spectrin and tau sensitize C. elegans axons to movement-induced damage via torque-tension coupling. *eLife*, 6(2010):e20172, 1 2017. ISSN 2050-084X. doi: 10.7554/eLife.20172. URL https://elifesciences.org/articles/20172.

K. L. Marshall and E. A. Lumpkin. The molecular basis of mechanosensory transduction. *Advances in Experimental Medicine and Biology*, 739:142–155, 2012. ISSN 00652598. doi: 10.1007/978-1-4614-1704-0{_}9.

A. L. Nekimken, H. Fehlauer, A. A. Kim, S. N. Manosalvas-Kjono, P. Ladpli, F. Memon, D. Gopisetty, V. Sanchez, M. B. Goodman, B. L. Pruitt, and M. Krieg. Pneumatic stimulation of C. elegans mechanoreceptor neurons in a microfluidic trap. *Lab Chip*, 17(6):1116–1127, 2017. ISSN 1473-0197. doi: 10.

1039/C6LC01165A. URL http://xlink.rsc.org/?DOI=C6LC01165Ahttp://dx.doi.org/10.1039/C6LC01165A.

R. O'Hagan. *Components of a Mechanotransduction Complex in C. elegans Touch Receptor Neurons: An in vivo Electrophysiology Study.* PhD thesis, Columbia University, 2005.

R. O'Hagan, M. Chalfie, and M. B. Goodman. The MEC-4 DEG/ENaC channel of Caenorhabditis elegans touch receptor neurons transduces mechanical signals. *Nature Neuroscience*, 8(1):43–50, 1 2005. ISSN 1097-6256. doi: 10.1038/nn1362. URL http://www.ncbi.nlm.nih.gov/pubmed/15580270http://www.nature.com/doifinder/10.1038/nn1362.

M. O'Toole, P. Lamoureux, and K. E. Miller. Measurement of subcellular force generation in neurons. *Biophysical Journal*, 108(5):1027–1037, 2015. ISSN 15420086. doi: 10.1016/j.bpj.2015.01.021.

B. C. Petzold, S.-J. Park, E. A. Mazzochette, M. B. Goodman, and B. L. Pruitt. MEMS-based force-clamp analysis of the role of body stiffness in C. elegans touch sensation. *Integrative biology : quantitative biosciences from nano to macro*, 5(6):853–864, 6 2013. doi: 10.1039/c3ib20293c. URL http://www.pubmedcentral.nih.gov/articlerender.fcgi?artid=3701114&tool=pmcentrez&rendertype=abstract.

A. J. Ribeiro, A. K. Denisin, R. E. Wilson, and B. L. Pruitt. For whom the cells pull: Hydrogel and micropost devices for measuring traction forces. *Methods*, 94:51–64, 2 2016. ISSN 10462023. doi: 10.1016/j.ymeth.2015.08.005. URL http://dx.doi.org/10.1016/j.ymeth.2015.08.005https://linkinghub.elsevier.com/retrieve/pii/S1046202315300438.

A. Sanzeni, S. Katta, B. Petzold, B. L. Pruitt, M. B. Goodman, and M. Vergassola. Somatosensory neurons integrate the geometry of skin deformation and mechanotransduction channels to shape touch sensing. *eLife*, 8:1–44, 2019. ISSN 2050-084X. doi: 10.7554/eLife.43226. URL https://elifesciences.org/articles/43226.

G. R. Sure, A. Chatterjee, N. Mishra, V. Sabharwal, S. Devireddy, A. Awasthi, S. Mohan, and S. P. Koushika. UNC-16/JIP3 and UNC-76/FEZ1 limit the density of mitochondria in C. elegans neurons by maintaining the balance of anterograde and retrograde mitochondrial transport. *Scientific Reports*, 8(1):8938, 12 2018. ISSN 2045-2322. doi: 10.1038/s41598-018-27211-9. URL http://www.nature.com/articles/s41598-018-27211-9.

H. Suzuki, R. Kerr, L. Bianchi, C. Frøkjær-Jensen, D. Slone, J. Xue, B. Gerstbrein, M. Driscoll, and W. R. Schafer. In Vivo Imaging of C. elegans Mechanosensory Neurons Demonstrates a Specific Role for the MEC-4 Channel in the Process of Gentle Touch Sensation. *Neuron*, 39(6):1005–1017, 9 2003. ISSN 08966273. doi: 10.1016/j.neuron.2003.08.015. URL http://linkinghub.elsevier.com/retrieve/pii/S0896627303005397.

B. E. Vogel and E. M. Hedgecock. Hemicentin, a conserved extracellular member of the immunoglobulin superfamily, organizes epithelial and other cell attachments into oriented line-shaped junctions. *Development*, 128(6):883–894, 2001. ISSN 0950-1991.

Q. Zheng, S. Ahlawat, A. Schaefer, T. Mahoney, S. P. Koushika, and M. L. Nonet. The Vesicle Protein SAM-4 Regulates the Processivity of Synaptic Vesicle Transport. *PLoS Genetics*, 10(10):e1004644, 10 2014. ISSN 1553-7404. doi: 10.1371/journal.pgen.1004644. URL `https://dx.plos.org/10.1371/journal.pgen.1004644`.

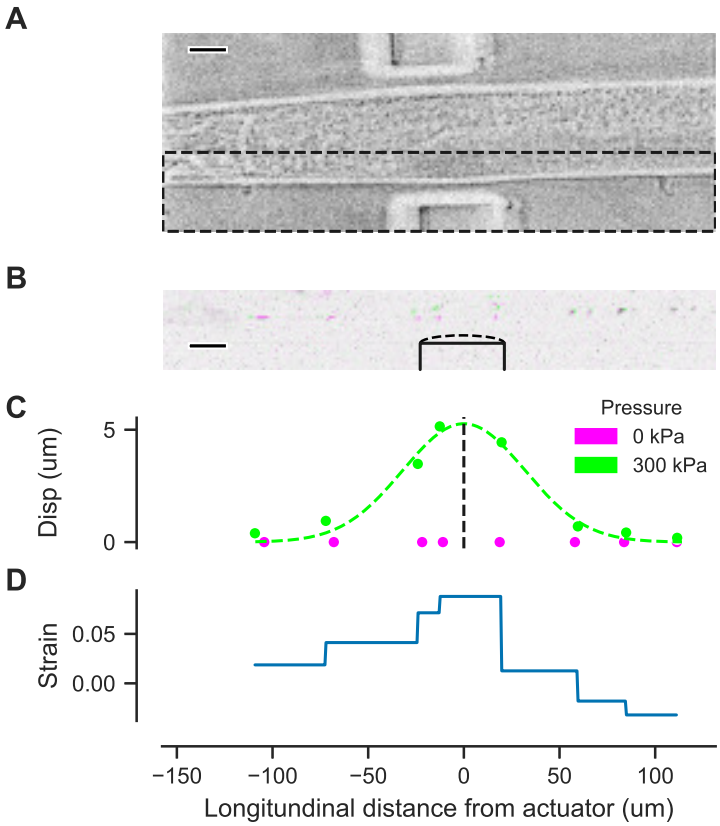

Figure 1: Touch-induced mechanical strain can be measured using mitochondria in *C. elegans* TRNs. A) Max projection of mitochondria in the TRN of a worm. B) Motion of mitochondria induced by mechanical stimulus. C) Displacement in the direction of actuation. With zero pressure applied, the displacement is zero by definition. Dotted line is fit of displacement to determine center of actuator. D) Distribution of touch-induced strain in the TRN for one actuation event.

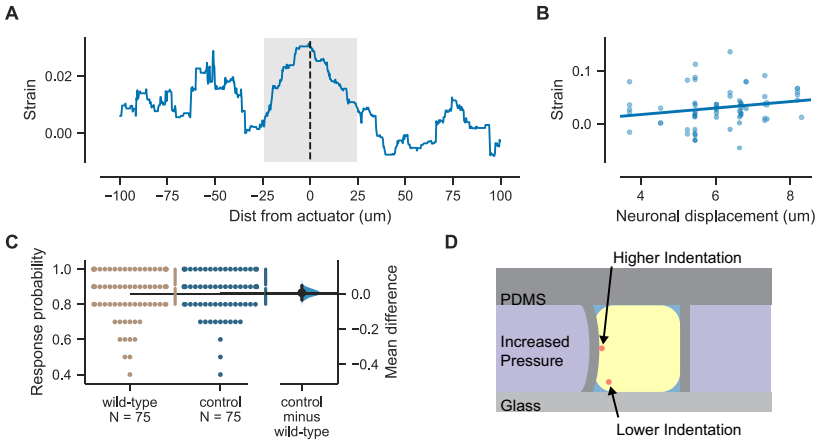

Figure 2: Indentation induces strain in *C. elegans* TRNs. A) Distribution of touch-induced strain in the TRN. The gray box indicates the location of the actuator channel. B) Touch-induced strain as a function of maximum interpolated displacement. The linear fit made with least-squares regression. C) Estimation plot of touch tests, showing that the transgenic mitochondria label in the TRN does not change touch sensitivity. The small lines next to the swarm plots indicate the median and quartiles of the data. The second axes show the difference in the mean response probability between N2 and transgenic worms with a bootstrapped resampled distribution of the data. D) Diagram showing differences in indentation for TRNs at different circumferential positions.

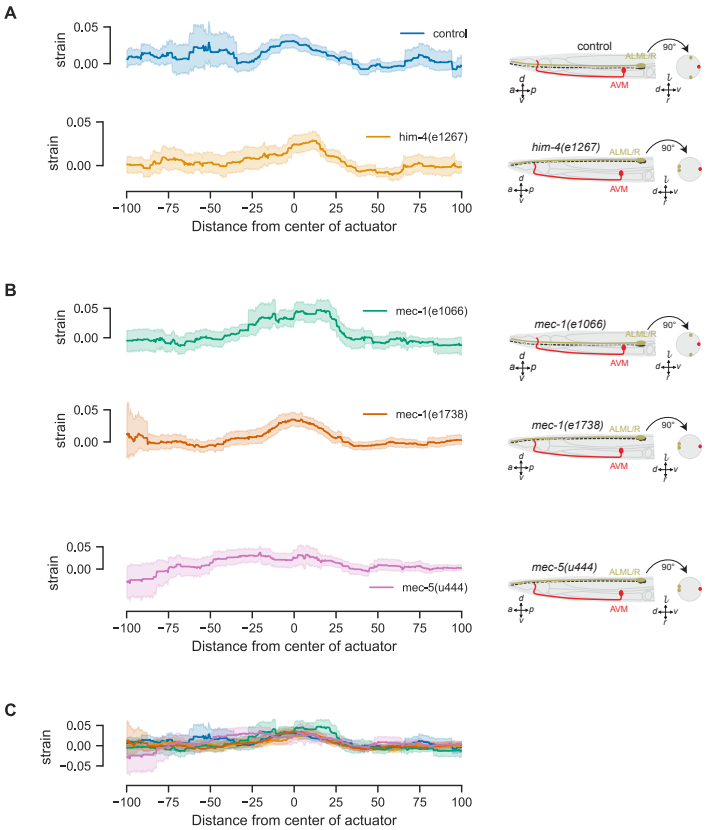

Figure 3: ECM mutations do not cause defects in transmission of mechanical strain. A) Spatially averaged strain in control and *him-4(e1267)*. The data for control animals are the same data as Figure 2. B) Spatially averaged strain in *mec-1* mutants with attachment defects (*mec-1(e1066)*) and without attachment defects (*mec-1(e1738)*). C) Spatially averaged strain in *mec-5(u444)* mutants. D) Overlay of all spatially averaged strain profiles.

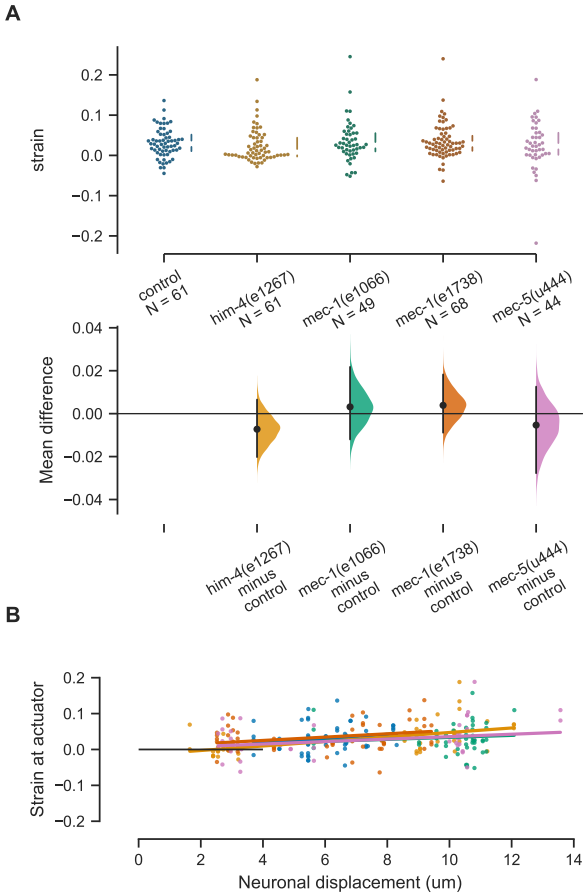

Figure 4: There is effectively no difference in transmission of mechanical between control animals and those with ECM mutations. A) Estimation plot of strain at the center of the actuator, and mean difference between control and mutant animals. The small lines next to the swarm plots indicate the median and quartiles of the data. The second axes show the difference in the mean strain between control and each mutant with a bootstrapped resampled distribution of the data. B) Strain at the center of the actuator vs. neuronal displacement (µm).

Genotype	Response probability	Mean difference from control	95% confidence interval of mean difference
Control	0.742		
him-4(e1267)	0.527	-0.215	(-0.275, -0.163)
mec-1(e1066)	0.083	-0.659	(-0.698, -0.619)
mec-1(e1738)	0.237	-0.505	(-0.551, -0.461)
mec-5(u444)	0.208	-0.534	(-0.580, -0.487)

Table 1: Touch sensitivity of ECM mutants. All mutants we tested were less sensitive to touch than control animals. All strains tested contained the transgene *jsIs1073*.

Genotype	Mean strain ±SEM	Mean difference from control	95% confidence interval of mean difference	Number of actuation events
Control	0.031 ±0.005			61
him-4(e1267)	0.024 ±0.005	-0.007	(-0.020, 0.007)	61
mec-1(e1066)	0.034 ±0.007	0.003	(-0.012 0.022)	49
mec-1(e1738)	0.035 ±0.005	0.004	(-0.009 0.018)	68
mec-5(u444)	0.026 ±0.009	-0.005	(-0.028 0.013)	44

Table 2: Strain transmission to TRNs of ECM mutants. There was effectively no difference in the magnitude of strain transmitted to the TRNs of ECM mutants as compared to control animals.

Strain Name	Genotype	Source
N2	wild-type	CGC
NM3573	jsIs1073	Nonet lab [Zheng et al., 2014]
GN885	jsIs1073;him-4(e1267)	cross NM3573 and CB1267
GN886	jsIs1073;mec-1(e1066)	cross NM3573 and CB1066
GN887	jsIs1073;mec-1(e1738)	cross NM3573 and CB3206
GN906	jsIs1073;mec-5(u444)	cross NM3573 and TU2969

Table 3: Worm strains used in this study.

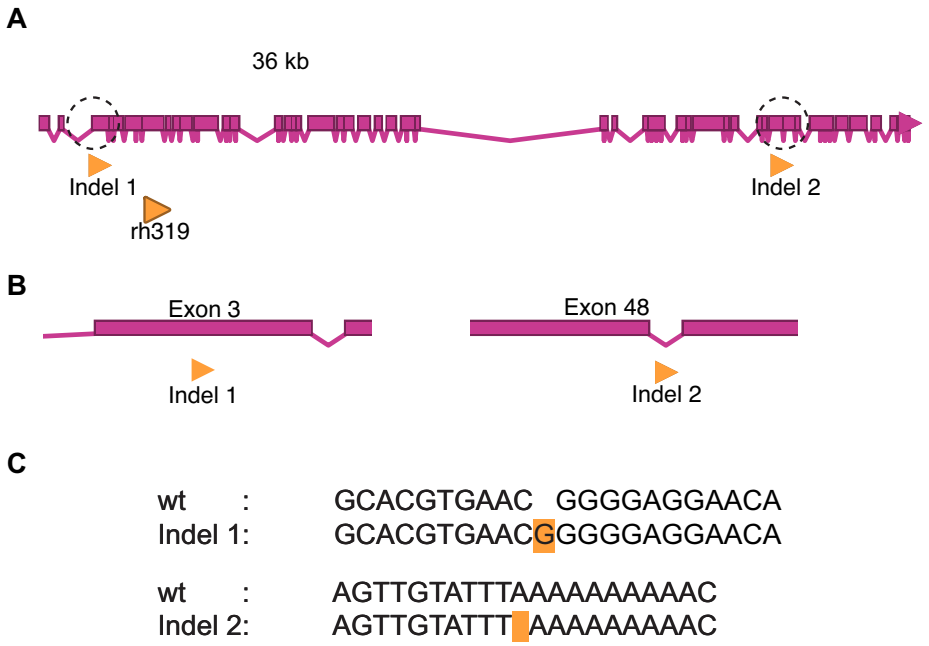

Figure S1: *him-4(e1267)* is likely to be a null allele. A) Map of *him-4* with *e1267* allele annotated. B) Close-up of insertion in sequence as indicated by dotted lines in Panel A. C) Sequences of both Indels found by sequencing. The first indel is likely to cause the null phenotype because it causes a frame-shift in an early exon, whereas the second indel is in a later intron.

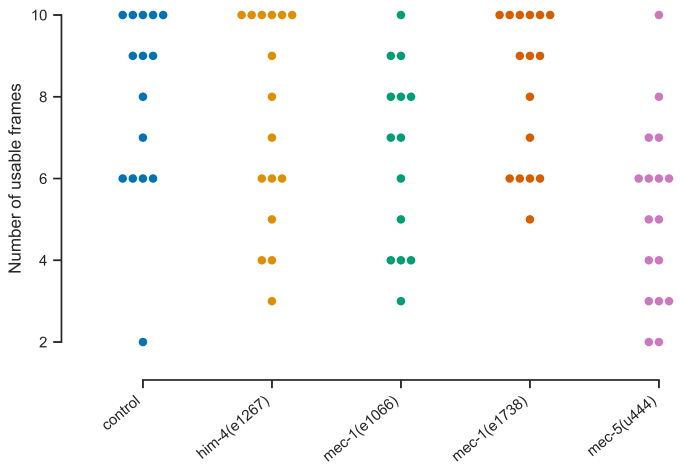

Figure S2: Not all z-stacks in each trial were usable. Note that we never used the 11th stack acquired in each experiment, since each strain measurement requires comparing the deformed configuration to the previous rest configuration. The 11th stack was always in the undeformed configuration with no subsequent stack in the deformed condition.

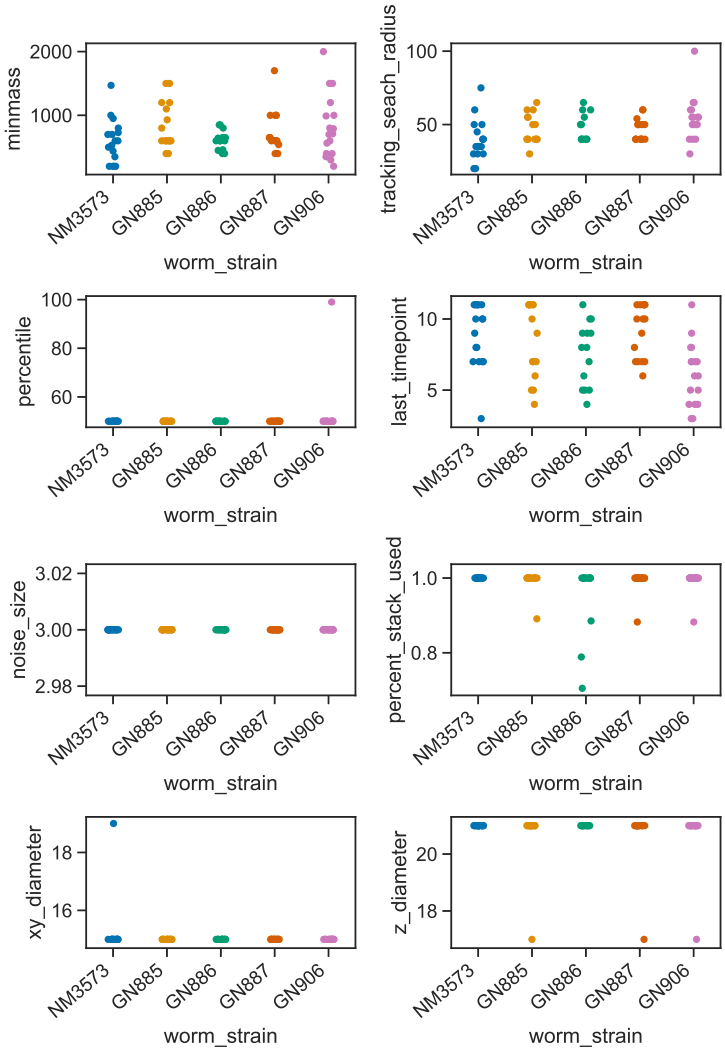

Figure S3: We tuned parameters of the particle tracking algorithm to account for variability across images.

Genotype	Mean distance ±SEM (µm)	Mean difference from control (µm)	95% confidence interval of mean difference (µm)	Minimum (µm)	Maximum (µm)
Control	26.0 ±0.4			5.0	64.4
him-4(e1267)	27.7 ±0.4	1.77	(0.6, 2.9)	5.0	76.1
mec-1(e1066)	27.2 ±0.5	1.2	(-0.1, 2.5)	4.7	67.3
mec-1(e1738)	26.6 ±0.4	0.7	(-0.5, 1.8)	5.1	64.1
mec-5(u444)	30.9 ±0.6	4.9	(3.5, 6.5)	5.4	84.8

Table S1: Estimation statistics for comparing distances between detected mitochondria compared to control animals. There is no significant difference between the mean distances of control and either *mec-1* allele, a small difference between the mean distance for *him-4(e1267)* animals, and a difference of nearly 5 m between the mean distances of control and *mec-5(u444)* animals.

Genotype	Mean number detected ±SEM	Mean difference from control	95% confidence interval of mean difference	Minimum	Maximum
Control	8.9 ±0.6			5	15
him-4(e1267)	9.1 ±0.5	0.2	(-1.5, 1.6)	6	13
mec-1(e1066)	8.8 ±0.5	-0.1	(-1.7, 1.5)	6	13
mec-1(e1738)	8.9 ±0.5	0.01	(-1.6, 1.5)	6	15
mec-5(u444)	7.2 ±0.5	-1.7	(-3.3, -0.3)	5	12

Table S2: Estimation statistics for comparing the number of detected mitochondria compared to control animals. There is no significant difference between the number of detected mitochondria of control and *him-4(e1267)*, *mec-1(e1066)*, or *mec-1(e1738)*. For *mec-5(u444)* animals, we detected 1.7 fewer mitochondria, on average.

Mutant Allele	Forward primer	Reverse primer	Sequencing primer
mec-1(e1066)	CATCTTCCACGCCGCAAAGTC	AATCCTCTCTGCCCTCATGTTCC	CGATAATTTTGTGGCAGCAGG
mec-1(e1738)	TCACAGTCAGACGTGCCTCG	CATTGCCTCACACCAACTTCCAC	GGCTGCGGAGGAAATCGAAATAG
mec-5(u444)	CAGAATACTATGTACGTAACTTGGGATC	CTCATGGGTACGCAAATGATACTC	N/A, gel for deletion screening
him-4(e1267)	TTTCGTGATGACTGGTGACTGTGG	TTAAAGTCAACAGCACCGTGACC	same as forward primer

Table S3: Primers used to confirm mutations after crosses. Note that *mec5(u444)* is a deletion mutant, so we used gel electrophoresis instead of sequencing to confirm the presence of the mutation.